

# Bound-State Spectra of a Lifshitz-Type Dirac Equation in (2+1) Dimensions

Lucas K. R. Queiroz,<sup>\*</sup> Van Sérgio Alves,<sup>†</sup> and Nilberto Bezerra<sup>‡</sup>  
*Faculdade de Física, Universidade Federal do Pará,  
Avenida Augusto Corrêa 01, 66075-110, Belém, Pará, Brazil*

Luis Fernández<sup>§</sup> and Francisco Peña<sup>¶</sup>  
*Departamento de Ciencias Físicas, Facultad de Ingeniería y Ciencias,  
Universidad de La Frontera, Avenida Francisco Salazar 01145, Casilla 54-D, Temuco Chile*  
(Dated: May 12, 2026)

We investigate a Dirac-type equation in (2+1) dimensions modified by Lifshitz spatial derivatives with dynamical exponent  $z = 2$ , focusing on the spectral properties of bound states under radial confinement. Analytical solutions are obtained for constant backgrounds, hard-wall confinement, and harmonic potentials, while logarithmic confinement is treated numerically via the Numerov method and complemented by a semiclassical WKB analysis. The resulting spectra exhibit characteristic scaling laws governed by the Lifshitz parameter  $b$ , including  $E - M \propto b/R_0^2$  for hard-wall confinement,  $E - M \propto \sqrt{2b}\omega$  for harmonic trapping, and  $E - M \sim \alpha \ln \sqrt{b}$  in the semiclassical regime of logarithmic confinement. These results provide a consistent characterization of how higher-order spatial derivatives modify bound-state spectra in two-dimensional Dirac systems and may be relevant for effective descriptions of materials with quadratic low-energy dispersion, such as bilayer graphene and related anisotropic 2D systems.

## I. INTRODUCTION

The Dirac equation provides the fundamental quantum description of spin-1/2 particles and has played a central role in modern physics since its formulation in 1928 [1]. Among its landmark achievements are the prediction of antiparticles [2] and the establishment of the theoretical foundations of quantum electrodynamics [3, 4]. In condensed-matter physics, Dirac-like Hamiltonians also emerge as effective low-energy descriptions, giving rise to quasiparticles with relativistic or quasi-relativistic behavior.

Since the experimental isolation of graphene in 2004, genuinely two-dimensional crystals have become experimentally accessible and controllable. In monolayer graphene, low-energy quasiparticles near the Dirac points behave as massless Dirac fermions in (2 + 1) dimensions, providing one of the clearest realizations of relativistic-like dynamics in condensed-matter systems [5, 6]. In transition-metal dichalcogenides such as MoS<sub>2</sub> and WS<sub>2</sub>, a massive Dirac structure arises together with spin-valley coupling and strong spin-orbit effects [7]. In bilayer graphene, by contrast, the low-energy spectrum is approximately quadratic in momentum, and the corresponding effective description departs from Lorentz-invariant linear dispersion [8]. These examples show that low-dimensional quantum materials provide experimentally accessible settings in which both Dirac-like dynamics and controlled departures from it can be explored.

Within an effective field theory (EFT) framework, departures from Lorentz invariance may arise from intrinsic anisotropies, lattice effects, or proximity to critical regimes with nontrivial scaling behavior. A natural way to parameterize such departures is through Lifshitz scaling, under which space and time transform anisotropically as  $x \rightarrow \lambda x$  and  $t \rightarrow \lambda^z t$ , where  $z$  is the dynamical critical exponent. The relativistic case corresponds to  $z = 1$ , whereas  $z \neq 1$  characterizes anisotropically scaled systems commonly encountered in condensed-matter contexts [9, 10]. Lifshitz-type extensions therefore provide a natural framework for describing nonrelativistic or anisotropic dispersion relations in two-dimensional systems.

In this work, we investigate the spectral properties of a Dirac-type equation in (2+1) dimensions modified by Lifshitz spatial derivatives with dynamical exponent  $z = 2$ . Our main goal is to determine how the Lifshitz deformation affects bound-state spectra under radial confinement. To this end, we combine analytical solutions for benchmark potentials with numerical calculations based on the Numerov method and a semiclassical WKB analysis. This unified approach allows us to identify characteristic scaling laws for the energy levels in different confinement regimes.

From an effective field theory perspective, such results help clarify how higher-order spatial derivatives modify spectral properties in two-dimensional Dirac systems and may be relevant for low-energy descriptions of materials with quadratic dispersion, such as bilayer graphene and related anisotropic 2D systems. Despite the broad literature on Lifshitz-type field theories, the spectral properties of confined Dirac-Lifshitz systems remain comparatively unexplored.

The paper is organized as follows. In Sec. II, we introduce the Lifshitz-type Dirac equation and derive

<sup>\*</sup> lucas.queiroz@icen.ufpa.br

<sup>†</sup> vansergi@ufpa.br

<sup>‡</sup> jose.bezerra@icen.ufpa.br

<sup>§</sup> luis.fernandez@ufrontera.cl

<sup>¶</sup> Deceased

the stationary Hamiltonian. In Sec. III, we analyze the constant-potential case and radial hard-wall confinement. In Sec. IV, we solve the harmonic-confinement problem and obtain the corresponding energy spectrum. In Sec. V, we study logarithmic confinement numerically through the Numerov method and analytically through a semiclassical WKB treatment. Finally, in Sec. VI, we summarize our main results and discuss possible extensions. In Appendix A, we transform the logarithmic problem into a form suitable for the Numerov and WKB methods.

## II. THE MODEL

We consider a Dirac-type equation in (2+1) dimensions modified by Lifshitz spatial derivatives, which explicitly break Lorentz invariance through higher-order spatial operators. The model is defined by

$$[i\gamma^0\partial_0 + b(i\gamma^i\partial_i)^z - M]\psi = 0, \quad (1)$$

where  $\gamma^\mu$  are Dirac matrices in a  $2 \times 2$  representation,  $b$  is a deformation parameter with dimensions  $[b] = [\text{mass}]^{1-z}$ ,  $M$  is a mass scale, and  $\psi$  is a two-component spinor field. Throughout this work, we adopt the representation  $(\gamma^0, \gamma^1, \gamma^2) = (\sigma_z, \sigma_x, \sigma_y)$ , where  $\sigma_i$  are the Pauli matrices. We restrict attention to the case  $z = 2$ , for which the higher-order spatial term produces a quadratic dependence on spatial derivatives, characteristic of Lifshitz-type dispersion. To obtain the stationary Hamiltonian, we multiply the equation by  $\gamma^0$  and use the Clifford algebra  $\{\gamma^i, \gamma^j\} = 2\delta^{ij}$ , which yields

$$(\gamma^i\partial_i)^2 = \nabla^2, \quad (2)$$

where  $\nabla^2 = \partial_1^2 + \partial_2^2$  is the two-dimensional Laplacian.

The equation of motion can then be written as

$$i\partial_0\psi = \gamma^0(b\nabla^2 + M)\psi. \quad (3)$$

Introducing an external scalar potential  $V(r)$ , the stationary Hamiltonian becomes

$$H = \gamma^0 [b\nabla^2 + M + V(r)], \quad (4)$$

which defines the eigenvalue problem  $H\psi = E\psi$ .

In the absence of external potentials, the model leads to the dispersion relation

$$E_\pm(k) = \pm (M + bk^2). \quad (5)$$

This dispersion differs from both the relativistic Dirac spectrum and the nonrelativistic Schrödinger form. In particular, the energy depends linearly on the mass scale while exhibiting a quadratic dependence on momentum, reflecting the underlying  $z = 2$  scaling. The spectrum should therefore be interpreted within an effective low-energy framework in which higher-order spatial derivatives encode departures from Lorentz-invariant dynamics.

To illustrate the qualitative features of this dispersion, we introduce an energy scale  $\Lambda$ . Consequently, the mass is expressed as  $u\Lambda$  (in units of  $\Lambda$ ), while the parameter  $b$  is written as  $u\Lambda^{-1}$  (in units of inverse  $\Lambda$ ). In this representation, the Lifshitz-type spectrum can be compared with the standard Schrödinger dispersion  $E_S(k) = k^2/2M$  and the relativistic Dirac spectrum  $E_D(k) = \pm\sqrt{k^2 + M^2}$ . As shown in Fig. 1, the Dirac-Lifshitz model exhibits symmetric energy branches separated by a finite gap  $2M$ , while displaying a quadratic momentum dependence distinct from both limiting cases.

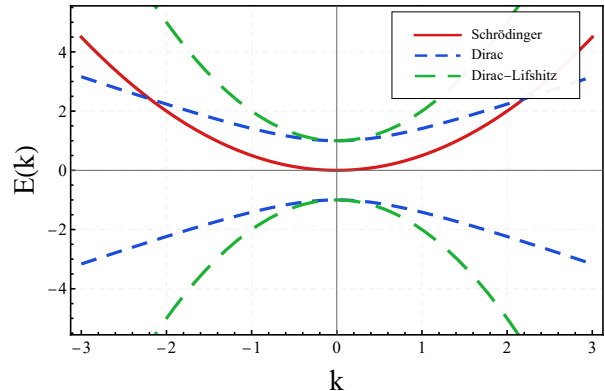


Figure 1. Qualitative representations of dispersion relations  $E(k)$  for the Schrödinger (red), Dirac (blue), and Dirac-Lifshitz (green) Hamiltonians. The parameters used were  $M = 1u\Lambda$  for all cases and  $b = 1u\Lambda^{-1}$ . The Dirac and Dirac-Lifshitz models show symmetric positive and negative branches separated by a finite gap  $|\Delta| = 2M$  at  $k = 0$ , while the Schrödinger case shows a single quadratic branch.

In two dimensions, such a quadratic dispersion leads to a density of states that differs qualitatively from the Dirac case. This feature suggests that the Lifshitz deformation captures effective regimes closer to systems with quadratic or anisotropic band structures, such as bilayer graphene or related materials [11–13].

For time-independent Hamiltonians, we separate temporal and spatial variables through the ansatz

$$\Psi(t, \mathbf{r}) = e^{-iEt}\psi(\mathbf{r}), \quad (6)$$

which reduces the problem to a stationary eigenvalue equation.

Since  $\gamma^0$  is diagonal in the chosen representation, its eigenvalues  $\lambda = \pm 1$  separate the spectrum into positive- and negative-energy branches. We therefore write the spinor as

$$\psi(\mathbf{r}) = \begin{pmatrix} \psi_+(\mathbf{r}) \\ \psi_-(\mathbf{r}) \end{pmatrix}. \quad (7)$$

We then apply separation of variables [14] and write the wave function as

$$\psi_\pm(\mathbf{r}) = R_\pm(r)\Phi(\phi). \quad (8)$$

We will omit the  $\pm$  subscripts to simplify the notation. In polar coordinates  $(r, \phi)$ , the Laplacian is

$$\nabla^2 = \frac{1}{r} \frac{\partial}{\partial r} \left( r \frac{\partial}{\partial r} \right) + \frac{1}{r^2} \frac{\partial^2}{\partial \phi^2}. \quad (9)$$

We use Eqs. (8) and (9) in Eq. (4) and obtain two independent equations, since the potential is radial. Then, the angular equation becomes the following

$$\frac{\partial^2 \Phi(\phi)}{\partial \phi^2} + l^2 \Phi(\phi) = 0, \quad (10)$$

with integer angular momentum  $l = \{0, \pm 1, \pm 2, \dots\}$ . Single-valuedness implies

$$\Phi_l(\phi) = A e^{il\phi}, \quad (11)$$

where  $A$  is a normalization constant.

On the other hand, the radial equation reads

$$b \left[ \frac{d^2 R}{dr^2} + \frac{1}{r} \frac{dR}{dr} - \frac{l^2}{r^2} R(r) \right] + [M + V(r) - E] R(r) = 0. \quad (12)$$

Equation (12) has the form of a Schrödinger-like radial equation with an energy-dependent effective potential. In the present case, however, the Lifshitz term modifies the kinetic sector itself, rather than reproducing the standard relativistic Dirac structure.

In the next section, we analyze the solution of Eq. (12) in two cases: at constant potential and for a finite potential well. Furthermore, we compare the radial solutions with those of the Schrödinger and Dirac equations.

### III. CONSTANT BACKGROUND AND RADIAL CONFINEMENT

#### A. Free particle and constant potential

We first consider a constant potential background,  $V(r) = V$ , which provides a simple analytically tractable reference case. In this situation, the radial equation reduces to

$$\frac{d^2 R}{dr^2} + \frac{1}{r} \frac{dR}{dr} - \frac{l^2}{r^2} R(r) + C R(r) = 0, \quad (13)$$

where

$$C = \sqrt{\frac{1}{b} (M + V - E)}. \quad (14)$$

The general solution is given in terms of Bessel functions,

$$R(r) = c_1 J_{|l|}(Cr) + c_2 Y_{|l|}(Cr), \quad (15)$$

where  $J_{|l|}$  and  $Y_{|l|}$  are Bessel functions of the first and second kinds, respectively. Regularity at the origin requires  $c_2 = 0$ , so that the physical radial solution becomes

$$R(r) = c_1 J_{|l|}(Cr). \quad (16)$$

To highlight the distinctive radial behavior of the model, we compare Eq. (16) for  $V = 0$  with the corresponding solutions of the radial Schrödinger and Dirac equations. In particular, we consider  $R_S(r) \sim J_{|l|}(k_S r)$  for the Schrödinger case and  $R_D(r) \sim J_{|l-1/2|}(k_D r)$  for the Dirac case, where  $k_S = \sqrt{2ME_S}$  and  $k_D = \sqrt{E_D^2 - M^2}$ , as shown in Fig. 2.

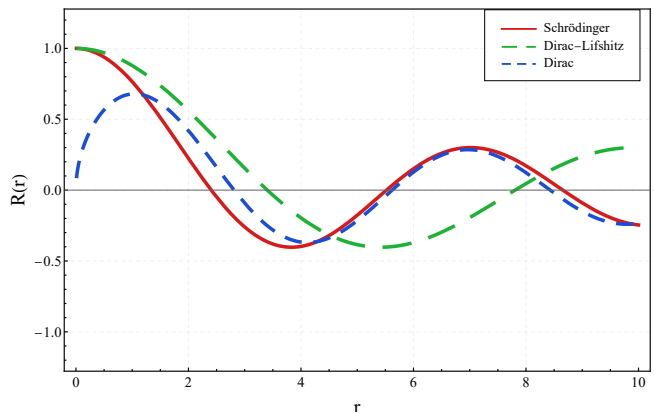


Figure 2. Comparison of the radial functions for each model with  $V = 0$ : The green curve corresponds to the Dirac-Lifshitz model, the red curve to the Schrödinger model, and the blue curve to the Dirac model. The chosen parameters are  $M = 1u\Lambda$  and  $l = 0$  in all cases;  $E = 0.5u\Lambda$  for the Dirac-Lifshitz and Schrödinger models;  $E_D = 1.5u\Lambda$  for the Dirac model; and for the Lifshitz parameter  $b = 1u\Lambda^{-1}$ . These choices allow for a direct comparison of their oscillatory structure.

As illustrated in Fig. 2, the Dirac-Lifshitz model displays an oscillatory radial structure whose node positions and characteristic scale are controlled by the parameter  $b$ . Although qualitative similarities with the Schrödinger and Dirac cases can be identified, the correspondence is not exact, especially in the presence of external potentials.

This behavior indicates that the Dirac-Lifshitz Hamiltonian defines a distinct spectral regime characterized by quadratic dispersion and a modified radial structure, rather than a simple interpolation between relativistic and nonrelativistic dynamics. Setting  $b = (M - E)/(2ME_S)$  recovers the Schrödinger curve, although qualitative similarities can be observed, the correspondence with these limiting regimes is not exact, particularly in the presence of external potentials.

This analysis highlights that the Dirac-Lifshitz Hamiltonian defines a distinct spectral regime characterized by quadratic dispersion and modified radial structure, rather than a simple interpolation between relativistic and nonrelativistic dynamics.

### B. Radial hard-wall confinement (“finite well” benchmark)

We now consider radial confinement inside a disk of radius  $R_0$ , implemented through hard-wall boundary conditions. This setup provides a simple benchmark for confined two-dimensional systems, such as quantum dots, in which the wave function vanishes at  $r = R_0$ .

Imposing the boundary condition  $R(R_0) = 0$  leads to the quantization condition

$$J_{|l|} \left( \sqrt{\frac{E-M}{b}} R_0 \right) = 0, \quad (17)$$

where  $l = \{0, \pm 1, \pm 2, \dots\}$  is the angular quantum number. Denoting by  $j_{l,n}$  the  $n$ -th zero of  $J_{|l|}$ , the energy spectrum is given by

$$E_{n,l} = M + b \left( \frac{j_{l,n}}{R_0} \right)^2. \quad (18)$$

The corresponding eigenfunctions take the form

$$\psi_{n,l}(t, r, \phi) = A_{n,l} J_{|l|} \left( \frac{j_{l,n}}{R_0} r \right) e^{il\phi} e^{-iE_{n,l}t}, \quad (19)$$

where  $A_{n,l}$  is a normalization constant.

A key feature of this spectrum is the scaling

$$E_{n,l} - M \propto \frac{b}{R_0^2}, \quad (20)$$

which directly reflects the anisotropic character of the Dirac-Lifshitz model. This quadratic dependence on the inverse confinement radius contrasts with the linear scaling typically found in massless Dirac systems. The result shows that the Lifshitz parameter  $b$  sets the confinement-induced energy scale and therefore provides a clear spectral signature of anisotropic scaling.

The eigenfunctions form a complete orthogonal set within the disk and can serve as a basis for the analysis of more general potentials or perturbations.

This benchmark also provides a useful point of comparison for smooth confining potentials, such as the harmonic oscillator considered in Sec. IV, where the quantization condition follows from the analytic structure of the wave function rather than from an imposed hard boundary.

## IV. HARMONIC OSCILLATOR

We now consider quadratic confinement described by the harmonic potential

$$V(r) = \frac{1}{2} \omega^2 r^2. \quad (21)$$

This potential provides a useful reference model for smooth confinement in two-dimensional systems and still

allows for an analytical treatment within the present framework. Substituting it into Eq. (12), and defining  $\kappa^2 = (E - M)/b$  and  $\Omega^2 = \omega^2/(2b)$ , we obtain

$$R''(r) + \frac{1}{r} R'(r) + \left[ \kappa^2 - \Omega^2 r^2 - \frac{l^2}{r^2} \right] R(r) = 0. \quad (22)$$

Introducing the dimensionless variable  $\rho = \sqrt{\Omega} r$ , the equation becomes

$$\frac{d^2 R}{d\rho^2} + \frac{1}{\rho} \frac{dR}{d\rho} + \left( \frac{\kappa^2}{\Omega} - \rho^2 - \frac{l^2}{\rho^2} \right) R(\rho) = 0. \quad (23)$$

The asymptotic behavior of Eq. (23) determines the structure of the physical solutions. For  $\rho \rightarrow 0$ , the centrifugal term dominates and yields  $R(\rho) \sim \rho^{|l|}$ , whereas for  $\rho \rightarrow \infty$  the harmonic term dominates and the solution decays as  $R(\rho) \sim e^{-\rho^2/2}$ .

These asymptotic behaviors motivate the ansatz

$$R(\rho) = \rho^{|l|} e^{-\rho^2/2} F(\rho). \quad (24)$$

Substituting this ansatz into Eq. (23), one finds that  $F(\rho)$  satisfies a confluent hypergeometric equation. Upon introducing the variable  $x = \rho^2$ , the equation becomes

$$xF''(x) + (|l| + 1 - x)F'(x) + \frac{1}{2} \left( \frac{\kappa^2}{\Omega} - 2|l| - 2 \right) F(x) = 0, \quad (25)$$

whose regular and normalizable solutions are the associated Laguerre polynomials  $L_n^{|l|}(x)$ , with  $n = \{0, 1, 2, \dots\}$ .

The normalized radial eigenfunctions are therefore given by

$$R_{n,l}(r) = N_{n,l} r^{|l|} \exp\left(-\frac{1}{2}\Omega r^2\right) L_n^{|l|}(\Omega r^2), \quad (26)$$

where  $N_{n,l}$  is a normalization constant. The requirement of polynomial solutions imposes the quantization condition

$$\frac{\kappa^2}{\Omega} = 2n + 2|l| + 2, \quad (27)$$

which determines the discrete spectrum.

This structure reflects the standard two-dimensional harmonic oscillator, where the radial quantum number effectively contributes as  $2n$  to the energy levels [15, 16].

Using the definitions of  $\kappa$  and  $\Omega$ , the energy spectrum is therefore given by

$$E_{n,l} = M + \sqrt{2b} \omega (2n + |l| + 1). \quad (28)$$

This result shows that the Lifshitz parameter  $b$  controls the level spacing through the effective scale  $\sqrt{2b}$ , reflecting the underlying  $z = 2$  anisotropic scaling. The harmonic case therefore provides a useful analytically solvable example of smooth confinement within the Dirac-Lifshitz framework.

## V. LOGARITHMIC CONFINEMENT: NUMERICAL SPECTRUM AND SEMICLASSICAL SCALING

We now consider the logarithmic confining potential

$$V(r) = \alpha \ln(r/r_0), \quad (29)$$

where  $\alpha$  sets the interaction strength and  $r_0$  defines a reference scale. Potentials of this type arise in effective low-dimensional descriptions and provide a useful setting for investigating semiclassical quantization.

Substituting this potential into the radial equation, we obtain

$$b \left[ R''(r) + \frac{1}{r} R'(r) - \frac{l^2}{r^2} R(r) \right] + [M + \alpha \ln(r/r_0) - E] R(r) = 0. \quad (30)$$

We solve this equation numerically using the Numerov method [17] and compare the resulting spectrum with a semiclassical WKB approximation [18]. We apply the transformation  $R(r) = u(r)/\sqrt{r}$ , to remove the first-derivative term and cast the radial equation into a Schrödinger-like form; we obtain the following equation,

$$\frac{d^2 u}{dr^2} + Q(r) u(r) = 0, \quad (31)$$

where

$$Q(r) = \frac{1}{b} [E - M - \alpha \ln(r/r_0)] - \frac{l^2 - 1/4}{r^2}. \quad (32)$$

Details of this reduction are given in the Appendix A.

### A. Numerov method

The reduced radial equation is solved numerically with the Numerov method, which is particularly suitable for second-order differential equations of the form  $u''(r) + Q(r)u(r) = 0$  with sufficiently smooth  $Q(r)$ .

The discretized recurrence relation is given by

$$u_{i+1} = \frac{\left(2 + \frac{5\tau^2}{6} Q_i\right) u_i - \left(1 - \frac{\tau^2}{12} Q_{i-1}\right) u_{i-1}}{1 - \frac{\tau^2}{12} Q_{i+1}}, \quad (33)$$

where  $\tau$  denotes the radial step size and  $Q_i = Q(r_i; E, l)$ .

The eigenvalues are determined through a shooting procedure by selecting solutions that remain finite near the origin and decay at large distances [19]. The radial function is normalized according to

$$\int_0^\infty |R(r)|^2 r dr = 1. \quad (34)$$

In the numerical implementation, the radial domain is chosen large enough to ensure convergence of the bound-state eigenvalues. The resulting discrete spectrum for  $l = 0$  is shown in Fig. 3.

### B. WKB quantization and Lifshitz scaling law

To obtain analytical insight into the spectrum, we employ a semiclassical WKB approximation. The corresponding quantization condition reads [20]

$$\int_{r_-}^{r_+} \sqrt{Q(r)} dr = \pi \left( n + \frac{1}{2} \right), \quad (35)$$

where  $n = \{0, 1, 2, \dots\}$  and  $r_\pm$  are the classical turning points. In WKB, the region  $Q(r) > 0$  corresponds to oscillatory solutions (classically allowed region), while  $Q(r) < 0$  corresponds to exponential decay.

In the large- $n$  regime, the centrifugal term may be neglected to leading order [18, 21], yielding

$$I(E) = \int_{r_-}^{r_+} \sqrt{\frac{1}{b} [E - M - \alpha \ln(r/r_0)]} dr. \quad (36)$$

This approximation becomes asymptotically accurate for highly excited states, for which the turning points occur at sufficiently large  $r$  and the logarithmic potential dominates over the centrifugal contribution.

Introducing the change of variable

$$s = E - M - \alpha \ln(r/r_0), \quad (37)$$

we obtain

$$r = r_0 \exp\left(\frac{E - M - s}{\alpha}\right), \quad (38)$$

and consequently

$$dr = -\frac{r_0}{\alpha} \exp\left(\frac{E - M - s}{\alpha}\right) ds. \quad (39)$$

Substituting Eqs. (37)–(39) into Eq. (36) leads to

$$I(E) = \frac{r_0}{\alpha\sqrt{b}} \exp\left(\frac{E - M}{\alpha}\right) \int_0^{E-M} s^{1/2} e^{-s/\alpha} ds. \quad (40)$$

The remaining integral has the structure of an incomplete gamma function. Introducing  $L = E - M$ , it can be written as

$$J_{\text{exact}} = \int_0^L s^{1/2} e^{-s/\alpha} ds = \alpha^{3/2} \gamma\left(\frac{3}{2}, \frac{L}{\alpha}\right), \quad (41)$$

where  $\gamma(a, x)$  denotes the lower incomplete gamma function. In the semiclassical regime, corresponding to large radial quantum numbers  $n \gg 1$ , the energy satisfies  $L = E - M \gg \alpha$ . Under this condition, the exponential factor  $\exp(-s/\alpha)$  decays rapidly, and the integral is dominated by values  $s \sim \alpha$ . Consequently, extending the upper integration limit to infinity introduces only a small error. The integral can therefore be approximated by

$$J_{\text{approx}} = \int_0^\infty s^{1/2} e^{-s/\alpha} ds = \alpha^{3/2} \Gamma(3/2). \quad (42)$$

The difference between the exact and approximate integrals corresponds to the tail contribution

$$\Delta J = J_{\text{approx}} - J_{\text{exact}} = \int_L^\infty s^{1/2} e^{-s/\alpha} ds. \quad (43)$$

This term can be expressed in terms of the upper incomplete gamma function [22],

$$\Delta J = \alpha^{3/2} \Gamma\left(\frac{3}{2}, \frac{L}{\alpha}\right). \quad (44)$$

For large arguments,  $x = L/\alpha \gg 1$ , the upper incomplete gamma function admits the asymptotic expansion

$$\Gamma(a, x) \sim x^{a-1} e^{-x} [1 + \mathcal{O}(1/x)]. \quad (45)$$

Applying this result with  $a = 3/2$ , the relative error of the approximation becomes

$$\frac{\Delta J}{J_{\text{approx}}} \sim \frac{2}{\sqrt{\pi}} \left(\frac{L}{\alpha}\right)^{1/2} \exp\left(-\frac{L}{\alpha}\right), \quad (46)$$

which is exponentially small. Therefore, extending the upper integration limit to infinity is an excellent approximation in the semiclassical regime, consistently with the Laplace-method estimate [22]. Performing this extension in Eq. (40), we obtain the approximate expression

$$I(E) \approx \frac{r_0}{2} \exp\left(\frac{E-M}{\alpha}\right) \sqrt{\frac{\alpha\pi}{b}}. \quad (47)$$

Returning to Eq. (35),

$$\frac{r_0}{2} \exp\left(\frac{E-M}{\alpha}\right) \sqrt{\frac{\alpha\pi}{b}} = \pi \left(n + \frac{1}{2}\right). \quad (48)$$

Solving for  $E$  yields the semiclassical scaling law

$$E_n \approx M + \alpha \ln \left[ \frac{2}{r_0} \sqrt{\frac{\pi b}{\alpha}} \left(n + \frac{1}{2}\right) \right]. \quad (49)$$

This result predicts a logarithmic growth of the energy levels,  $E_n - M \sim \alpha \ln \sqrt{b}$ , in agreement with the numerical solutions obtained via the Numerov method, as shown in Fig. 3.

Figure 3 compares the numerical spectrum obtained with the Numerov method with the semiclassical prediction in Eq. (49). For sufficiently large radial cutoffs, the two approaches are in very good agreement over the range of quantum numbers considered. In both cases, the spectrum exhibits the characteristic logarithmic growth associated with the confining nature of the potential.

To quantify this agreement, we evaluate the relative error  $\epsilon = (E_{\text{Numerov}} - E_{\text{WKB}})/E_{\text{Numerov}}$  as a function of the radial quantum number  $n$ . The results, shown in Fig. 4, identify the regime in which the WKB approximation provides an accurate description of the spectrum, as well as the range in which noticeable deviations persist.

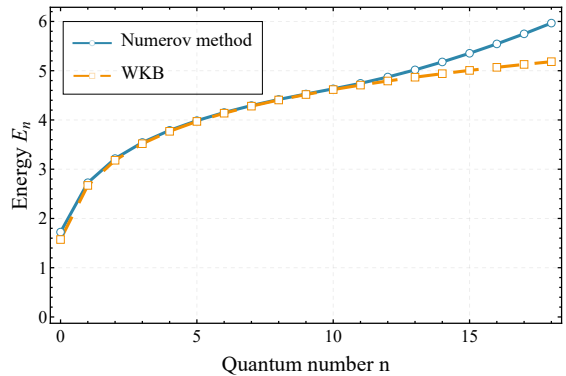


Figure 3. Comparison between the numerical spectrum obtained with the Numerov method and the semiclassical prediction of Eq. (49) for  $l = 0$ ,  $b = 1u\Lambda^{-1}$ ,  $\alpha = 1u\Lambda$ ,  $r_0 = 1u\Lambda^{-1}$  and  $M = 1u\Lambda$ . The radial cutoff was chosen sufficiently large to ensure the proper decay of the wave functions for highly excited states.

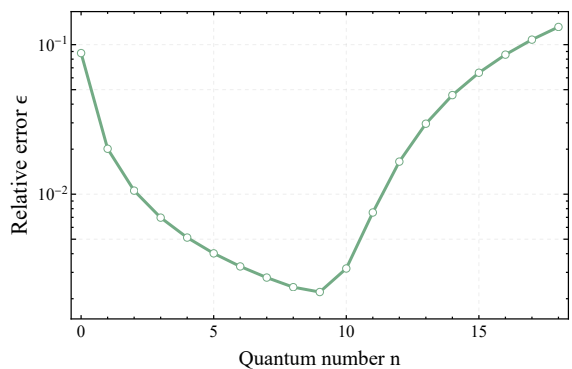


Figure 4. Relative error between the eigenvalues obtained with the Numerov method and the semiclassical estimate given by Eq. (49). The deviation is largest for the lowest state  $n = 0$  and for large  $n$ , where semiclassical approximations are not expected to be reliable. As the quantum number increases the agreement improves, reaching a minimum error around  $n = 9$ . For higher states the error slowly increases again, which can be attributed to the growing spatial extent of the excited states and the finite radial cutoff used in the numerical integration.

Having verified that the WKB approximation accurately reproduces the numerical spectrum for  $l = 0$ , we now extend the analysis to states with nonzero angular momentum. In this case, the centrifugal term modifies the effective potential, as shown in Eq. (32), and is expected to affect the semiclassical quantization condition. Guided by the structure of radial WKB methods, we introduce an effective shift in the quantum number  $n \rightarrow n + c_l$ , where  $c_l$  is determined by fitting the WKB expression to the numerical spectrum for  $l \neq 0$ .

This procedure effectively incorporates the contribution of the centrifugal term, which is not fully captured by the leading-order logarithmic approximation. We find that the semiclassical spectrum can be significantly improved by incorporating an effective shift in the radial quantum number, leading to the expression

$$E_{n,l} \approx M + \alpha \ln \left[ \frac{2}{r_0} \sqrt{\frac{\pi b}{\alpha}} \left( n + \frac{|l|}{2} + \frac{3}{4} \right) \right]. \quad (50)$$

This form provides an excellent agreement with the numerical results obtained via the Numerov method, with only small deviations for the lowest the highest angular momentum states.

## VI. CONCLUSIONS AND OUTLOOK

We have investigated the spectral properties of a Dirac-type equation in  $(2+1)$  dimensions modified by Lifshitz spatial derivatives with dynamical exponent  $z = 2$ , with emphasis on bound states under radial confinement. The higher-order spatial term produces a quadratic dispersion relation and, consequently, systematic departures from Lorentz-invariant Dirac dynamics.

Analytical solutions were obtained for constant backgrounds, hard-wall confinement, and harmonic potentials, whereas logarithmic confinement was studied through a combination of Numerov-based numerical calculations and a semiclassical WKB analysis. Across these regimes, the energy spectrum exhibits characteristic scaling laws, including  $(E - M) \propto b/R_0^2$  for hard-wall confinement,  $E - M \propto \sqrt{2b}\omega$  for harmonic trapping, and  $E - M \sim \alpha \ln \sqrt{b}$  for logarithmic confinement in the semiclassical regime. The agreement between the numerical and semiclassical results supports the consistency of these spectral behaviors.

From an effective field theory perspective, these results provide a consistent characterization of how Lifshitz-type modifications affect bound-state spectra in two-dimensional Dirac systems. Such behavior may be relevant for effective descriptions of systems with parabolic or anisotropic low-energy dispersion.

Future work may extend the present analysis by incorporating external fields, boundary effects, and interactions, which may help clarify the role of Lifshitz-type operators in more realistic two-dimensional settings.

## ACKNOWLEDGMENTS

L. K. Q. and N. B. were partially supported by the Coordenação de Aperfeiçoamento de Pessoal de Nível

Superior (CAPES). V. S. A. was partially supported by the Conselho Nacional de Desenvolvimento Científico e Tecnológico (CNPq-Brazil) through Process No. 408735/2023-6 (CNPq/MCTI). L. F. acknowledges financial support from the Vicerrectoría de Investigación y Postgrado de la Universidad de La Frontera through Project No. BPVRIP-092024. The authors dedicate this work to the memory of Francisco Peña, whose scientific insight, collaboration, and friendship were invaluable throughout this project.

## Appendix A: Details of the radial reduction

Starting from Eq. (4) and using polar coordinates, one arrives at Eq. (12) after separating variables. After applying the derivatives and renaming the radial functions, we arrive at Eq. (12). That way, we can make the transformation  $R(r) = u(r)/\sqrt{r}$ . This is the standard radial reduction used to transform the problem into a form suitable for the Numerov and WKB methods. Applying this transformation, we have for the first derivate

$$R' = \frac{d}{dr}(r^{-1/2}u) = -\frac{1}{2}r^{-3/2}u + r^{-1/2}u' \quad (A1)$$

and differentiating again,

$$R'' = \frac{3}{4}r^{-5/2}u - r^{-3/2}u' + r^{-1/2}u''. \quad (A2)$$

First, we compute

$$R'' + \frac{1}{r}R' = \left( \frac{3}{4}r^{-5/2}u - r^{-3/2}u' + r^{-1/2}u'' \right) + \left( -\frac{1}{2}r^{-5/2}u + r^{-3/2}u' \right), \quad (A3)$$

the first-derivative terms cancel, thus

$$R'' + \frac{1}{r}R' = \frac{1}{4}r^{-5/2}u + r^{-1/2}u''. \quad (A4)$$

Substituting into the Eq. (12), the radial equation becomes

$$\left( \frac{1}{4}r^{-5/2}u + r^{-1/2}u'' \right) - l^2 r^{-5/2}u + \frac{1}{b} [E - M - \alpha \ln(r/r_0)] r^{-1/2}u = 0, \quad (A5)$$

factoring out  $r^{-1/2}$ , the reduced equation for  $u(r)$  is Eq. (31). This transformation introduces the effective centrifugal term  $l^2 - 1/4$  in the Eq. (32), which is purely geometric and arises from the two-dimensional radial measure. This structure is analogous to the appearance of  $l(l+1)$  in three-dimensional radial problems [24].

- 
- [1] P. A. M. Dirac, “The quantum theory of the electron,” Proc. Roy. Soc. Lond. A **117**, 610 (1928).
- [2] C. D. Anderson, “The apparent existence of easily deflectable positives,” Science **76**, 238 (1932).
- [3] J. D. Bjorken and S. D. Drell, *Relativistic Quantum Mechanics*, McGraw-Hill, New York, (1965).
- [4] M. E. Peskin and D. V. Schroeder, *An Introduction to Quantum Field Theory*, CRC Press, Boca Raton, (2018).
- [5] K. S. Novoselov *et al.*, “Electric field effect in atomically thin carbon films,” Science **306**, 666 (2004).
- [6] A. H. Castro Neto, F. Guinea, N. M. R. Peres, K. S. Novoselov, and A. K. Geim, “The electronic properties of graphene,” Rev. Mod. Phys. **81**, 109 (2009).
- [7] X. Xu, W. Yao, D. Xiao, and T. F. Heinz, “Spin and pseudospins in layered transition metal dichalcogenides,” Nat. Phys. **10**, 343 (2014).
- [8] E. McCann and M. Koshino, “The electronic properties of bilayer graphene,” Rep. Prog. Phys. **76**, 056503 (2013).
- [9] R. M. Hornreich, M. Luban, and S. Shtrikman, “Critical behavior at the onset of  $\vec{k}$ -space instability on the  $\lambda$  line,” Phys. Rev. Lett. **35**, 1678 (1975).
- [10] P. Hořava, “Quantum gravity at a Lifshitz point,” Phys. Rev. D **79**, 084008 (2009).
- [11] M. I. Katsnelson and G. E. Volovik, “Quantum electrodynamics with anisotropic scaling: Heisenberg-Euler action and Schwinger pair production in bilayer graphene,” arXiv:1203.1578 [cond-mat.mes-hall] (2012).
- [12] V. N. Kotov, B. Uchoa, and O. P. Sushkov, “Coulomb interactions and renormalization of semi-Dirac fermions near a topological Lifshitz transition,” Phys. Rev. B **103**, 045403 (2021).
- [13] Y.-C. Lee, D. V. Chichinadze, and A. V. Chubukov, “Crossover from ordinary to higher order Van Hove singularity in a honeycomb system: A parquet renormalization group analysis,” Phys. Rev. B **109**, 155118 (2024).
- [14] D. J. Griffiths and D. F. Schroeter, *Introduction to Quantum Mechanics*, Cambridge University Press, Cambridge, (2018).
- [15] V. M. Villalba, “Exact solution of the two-dimensional Dirac oscillator,” Phys. Rev. A **49**, 586 (1994).
- [16] M. Moshinsky and A. Szczepaniak, “The Dirac oscillator,” J. Phys. A **22**, L817 (1989).
- [17] E. Hairer, S. P. Nørsett, and G. Wanner, *Solving Ordinary Differential Equations I: Nonstiff Problems*, Springer-Verlag, Berlin, (1993).
- [18] N. Fröman and P. O. Fröman, *JWKB Approximation*, North-Holland Publishing Company, Amsterdam, (1965).
- [19] J. M. Blatt, “Practical points concerning the solution of the Schrödinger equation,” J. Comput. Phys. **1**, 382 (1967).
- [20] B. R. Desai, *Quantum Mechanics with Basic Field Theory*, Cambridge University Press, Cambridge, (2010).
- [21] B. M. Karanakov and V. P. Krainov, *WKB Approximation in Atomic Physics*, Springer, Heidelberg, (2012).
- [22] C. M. Bender and S. A. Orszag, *Advanced Mathematical Methods for Scientists and Engineers: Asymptotic Methods and Perturbation Theory*, Springer, New York, (1999).
- [23] C. Quigg and J. L. Rosner, “Quantum mechanics with applications to quarkonium,” Phys. Rep. **56**, 167 (1979).
- [24] M. V. Berry and A. M. Ozorio de Almeida, “Semiclassical approximation of the radial equation with two-dimensional potentials,” J. Phys. A **6**, 1451 (1973).